PERGAMON

Journal of Quantitative Spectroscopy & Radiative Transfer 65 (2000) 543–571

Journal of Quantitative Spectroscopy & Radiative Transfer

www.elsevier.com/locate/jqsrt

Review of the advanced generalized theory for Stark broadening of hydrogen lines in plasmas with tables

J.E. Touma[a], E. Oks[a,*], S. Alexiou[a], A. Derevianko[b]

[a]*Department of Physics, Auburn University, 206 Allison Laboratory, Auburn, AL 36849-5311, USA*
[b]*Department of Physics, Notre Dame University, USA*

Abstract

The Generalized Theory (GT) of Stark broadening of Stark broadening of hydrogen lines in plasmas, published by Ispolatov and Oks (JQSRT 1994; 51:19-9-38) is based on nonperturbative treatment of one component of the electron field. Therefore the GT is intrinsically more accurate than the fully-perturbative, Standard Theories (ST), such as the theory by Kepple–Griem (Phys Rev 1968; 173:317–25) (KG) and the theory by Sholin-Demura-Lisitsa (Sov Phys JETP 1973; 37:1057–65) (SDL). The present paper introduces an Advanced Generalized Theory (AGT), that yields closed-form expressions for the width, shift and coupling of Stark states. We also present tables of the AGT Stark widths of Lyman and Balmer lines for transitions with upper levels having principal quantum numbers $n \leq 16$ and for electron densities from $N_e = 10^{13}$ cm^{-3} to $N_e = 10^{20}$ cm^{-3}. The mathematical simplicity of the AGT results make it possible to gain physical insight into the important features of the generalized theories that distinguish the AGT/GT from its predecessors. Empirical choices of important characteristic impact parameters made previously, are shown, using the insights possible with the AGT, to be inaccurate: (A) In the AGT, the effective Weisskopf radius ρ_W is proportional to n^2, while SDL had empirically chosen ρ_W proportional to n; (B) in the AGT, the effective Weisskopf radius ρ_W is defined for each Stark component (i.e., dependent on the electric quantum number q), while KG had empirically chosen a component-independent ρ_W; (C) in the AGT the ion-field-dependent upper cutoff ρ_F is proportional to $1/n$ while KG had empirically chosen an expression for ρ_F proportional to $1/n^2$. The AGT shows that in high fields or high density range, the coupling between the ion and electron broadenings is significantly stronger than proposed by both the KG and SDL theories. Even in the low field or low density range, where the coupling between the ions and electrons broadening is negligible, the results of the AGT are more accurate than the results of the Standard Theories. In addition to yielding the effective Weisskopf radius (as noted above), the AGT can evaluate the "strong collision constant" — in distinction to both the KG and SDL theories, where the choice of this constant is empirical. The comparison of the tabulated Stark widths with the KG Stark widths indicates that the inaccuracy of the KG width is significantly increased with the increasing electron density N_e and upper principal quantum number n.

* Corresponding author. Tel.: 001-334-844-4362.
E-mail address: goks@physics.auburn.edu (E. Oks)

PII: S0022-4073(99)00095-3

However, even for the L_α line at, e.g., densities 10^{17} cm^{-3} — where the experimental width is a factor of two greater than the calculated KG width and the entire difference between the two widths was usually attributed to the ion dynamics — it turns out that the AGT eliminates about one half of this discrepancy indicating that the ion-dynamical contribution is in reality about a factor of two smaller than it was previously assumed.

1. Introduction

The Generalized Theory (GT) of Stark broadening of hydrogen lines in plasmas was developed by Ispolatov and Oks [1] in 1994. The GT treats *non-perturbatively* both the ion produced field **F** and a projection $[\mathbf{E}(t)]_{\mathbf{F}}$ of the electron produced field $\mathbf{E}(t)$ onto the vector **F**. The other two projections of the electron field $[\mathbf{E}(t)]$ were treated in a second-order perturbation theory as in the Standard Theories (ST), such as Kepple–Griem's [2] (KG) and Sholin-Demura-Lisitsa's [3] (SDL).

By treating one component of the electron field "exactly", the GT eliminated the divergence at small impact parameters, which is intrinsic in the ST. It should be emphasized that the GT reduces to the ST in the case when both the electron density N_e and the upper principal quantum number n are relatively small. However, the inaccuracy of the ST is expected to grow as the electron density and (or) the upper principal quantum increase(s).

In the GT the angular integrations were performed analytically, as in the ST, and four integrations remained: two time-integrations, one integration over impact parameters and the final integration over the ion microfield F.

The integrands are strongly oscillating functions of all three variables. The numerical difficulties became the main motivation for the development of a more user-friendly form of the GT: The Advanced Generalized Theory (AGT).

In the AGT, we performed a $1/\chi$ expansion of our broadening functions allowing us to analytically perform the two time integrations exactly and the integration over impact parameters piece-wise. We define χ as $\chi \equiv X/n$ for the upper multiplet and $\chi' \equiv X/n'$ for the lower multiplet. Here X is the combination of parabolic quantum numbers that controls the static Stark shift of each component:

$$X \equiv nq - n'q', \quad q = n_1 - n_2, \quad q' = n'_1 - n'_2.$$

In the limit of large upper principal quantum numbers, $n \gg n'$, χ reduces to q: $\chi \approx q$. So, the expansion of the broadening functions was performed essentially for large electric quantum numbers. By comparing our analytical results with the exact numerical integration over impact parameters, we found that our analytical results have excellent accuracy for $\chi \gg 1$ with an accuracy of about 5% for $\chi = 1$.

The approach was different for values of $\chi < 1$, e.g., central unshifted Stark components. In the large ion field region, we derived the AGT results analytically using the steepest descent method where the result is significantly different from the ST. In the low ion field region, the AGT violates unitarity, as does the ST. So, in this region, we used the same unitarity based approximation as in the ST (for the central Stark components).

After the final integration over impact parameters, all the AGT's broadening functions depend only on one parameter, defined as

$$\kappa = \frac{9}{2}\left(\frac{\hbar}{m_e v}\right)^2 nXF \tag{1}$$

where F is the static ion field, $\hbar$ is Plank's constant, m_e is the electron mass and v is the electron velocity. Physically, κ is the reduced, or renormalized, static ion field.

2. Analytical results for the broadening functions

After performing the angular integrations, the GT yields the following for the electron impact operator:

$$\begin{aligned}\hat{\Phi} = & -\left(\frac{4\pi\hbar^2 N_e}{(3m_e^2 a_0^2)^2}\right)\int_0^\infty \mathrm{d}v\, W_M(v) v^{-1} \\ & \times\left\{(\hat{z}_a - \hat{z}_b^*)^2 \int_0^{u_{\max}} \mathrm{d}u\, 6u\left(1 - u\sin\frac{1}{u}\right)\right\} \\ & + (\hat{x}_a\hat{x}_a + \hat{y}_a\hat{y}_a)\int_0^{Z_{\max}} \frac{\mathrm{d}Z}{Z} C_a^{\pm}(\chi_a,\ Y_a,\ Z_a) \\ & + (\hat{x}_b^*\hat{x}_b^* + \hat{y}_b^*\hat{y}_b^*)\int_0^{Z_{\max}} \frac{\mathrm{d}Z}{Z} C_b^{\pm}(\chi_b,\ Y_b,\ Z_b) \\ & - \left\{2(\hat{x}_a\hat{x}_b^* + \hat{y}_a\hat{y}_b^*)\int_0^{Z_{\max}} \frac{\mathrm{d}Z}{Z} C_{\times}(\chi_a,\ Y_a,\ Y_b,\ Z_a,\ Z_b)\right\}\end{aligned} \tag{2}$$

where

$$u = \frac{\rho}{\rho_W^{ad}},\quad Z = \frac{\rho}{\rho_S},\quad \rho_W^{ad} = \frac{3X_{\alpha\beta}\hbar}{m_e v},\quad X_{\alpha\beta} = n_\alpha q_\alpha - n'_\beta q'_\beta,\quad \rho_s = \frac{2m_e e v}{3n_{\alpha,\beta}\hbar F}.$$

Here N_e is the electron density, ρ is the impact parameter of the perturbing electron, n is the principal quantum number, $q = n_1 - n_2$ is the electric quantum number (expressed via the parabolic quantum numbers), suffix α refers to the upper multiplet, and suffix β refers to the lower multiplet.

The first term in $\{\cdots\}$ is the adiabatic contribution to the impact operator and can be integrated analytically:

$$\int_0^{u_m} \mathrm{d}u\, 6u\left(1 - u\sin\frac{1}{u}\right) = 3u_m^2 - \left[u_m^2\cos\frac{1}{u_m} + (2u_m^3 - u_m)\sin\frac{1}{u_m} + \mathrm{Ci}\left(\frac{1}{u_m}\right)\right], \tag{3}$$

where $\mathrm{Ci}(x)$ is the integral cosine function.

The last three terms in $\{\cdots\}$ in Eq. (2) are the nonadiabatic part of the impact operator. The upper sign in Eq. (2) corresponds to the nondiagonal elements of the impact operator while the lower sign corresponds to the diagonal elements. As mentioned above, three integrations remained even before the final integration over the ion microfield. The two-time integrations are implicit in the functions $C_a^{\pm}$, $C_b^{\pm}$ and $C_{\times}$. The integration over impact parameters is explicit in the definition of the impact operator. The AGT is primarily concerned with obtaining analytical results for the nonadiabatic contribution to the impact operator to the line profile. Dropping the subscripts a and b and making $\pm$ a subscript, the functions $C_a^{\pm}$ and $C_b^{\pm}$ are given by

$$C_{\pm}(\chi, Y, Z) = \frac{3}{4}\int_{-\infty}^{\infty} dx_1 \int_{-\infty}^{x_1} dx_2 \frac{\exp[iZ(x_1 \pm x_2)]}{w^3(x_1)w^3(x_2)}\{j_0(\varepsilon)\} + \left\{(2x_1x_2 - 1)\frac{j_1(\varepsilon)}{\varepsilon} + [(1 - x_1x_2)\sigma_1^2 - (x_1 + x_2)\sigma_1\sigma_2]\frac{j_2(\varepsilon)}{\varepsilon^2}\right\} \tag{4}$$

where

$$\varepsilon = \sqrt{\sigma_1^2 + \sigma_2^2}, \tag{5}$$

$$\sigma_1 = \frac{Y}{Z}[x_1 w(x_1) - x_2 w(x_2) + 1 \pm 1 - 2\chi],$$

$$\sigma_2 = \frac{Y}{Z}[w(x_1) \pm w(x_2)], \quad w(x) = \sqrt{1 + x^2},$$

$$j_0(\varepsilon) = \varepsilon^{-1}\sin\varepsilon, \quad j_1(\varepsilon) = \varepsilon^{-2}(\sin\varepsilon - \varepsilon\cos\varepsilon),$$

$$j_2(\varepsilon) = \varepsilon^{-3}(3\sin\varepsilon - 3\varepsilon\cos\varepsilon - \varepsilon^2\sin\varepsilon)$$

(the latter three functions are the spherical Bessel functions). The variables x_1 and x_2 are the standard notation of the ST:

$$x_1 = vt_1/\rho, \quad x_2 = vt_2/\rho. \tag{6}$$

As for the interference term, we have

$$C_{\times}(\chi_a, Y_a, Y_b, Z_a, Z_b) = \frac{3}{4}\int_{-\infty}^{\infty} dx_1 \int_{-\infty}^{\infty} dx_2 \frac{\exp[Z_\beta x_2 - Z_\alpha x_1]}{w^3(x_1)w^3(x_2)} \times \left\{j_0(\varepsilon) + (2x_1x_2 - 1)\frac{j_1(\varepsilon)}{\varepsilon} + [(1 - x_1x_2)\sigma_1^2 - (x_1 + x_2)\sigma_1\sigma_2]\frac{j_2(\varepsilon)}{\varepsilon^2}\right\} \tag{7}$$

where

$$\varepsilon = \sqrt{\sigma_1^2 + \sigma_2^2}, \tag{8}$$

$$\sigma_1 = 2\chi_\alpha\frac{Y_\alpha}{Z_\alpha} + \left(1 + \frac{x_2}{\sqrt{1 + x_2^2}}\right)\frac{Y_\beta}{Z_\beta} - \left(1 + \frac{x_1}{\sqrt{1 + x_1^2}}\right)\frac{Y_\alpha}{Z_\alpha}, \tag{9}$$

$$\sigma_2 = \frac{1}{\sqrt{1 + x_1^2}}\frac{Y_\alpha}{Z_\alpha} - \frac{1}{\sqrt{1 + x_2^2}}\frac{Y_\beta}{Z_\beta}. \tag{10}$$

The variables x_1 and x_2 are given by Eq. (6).

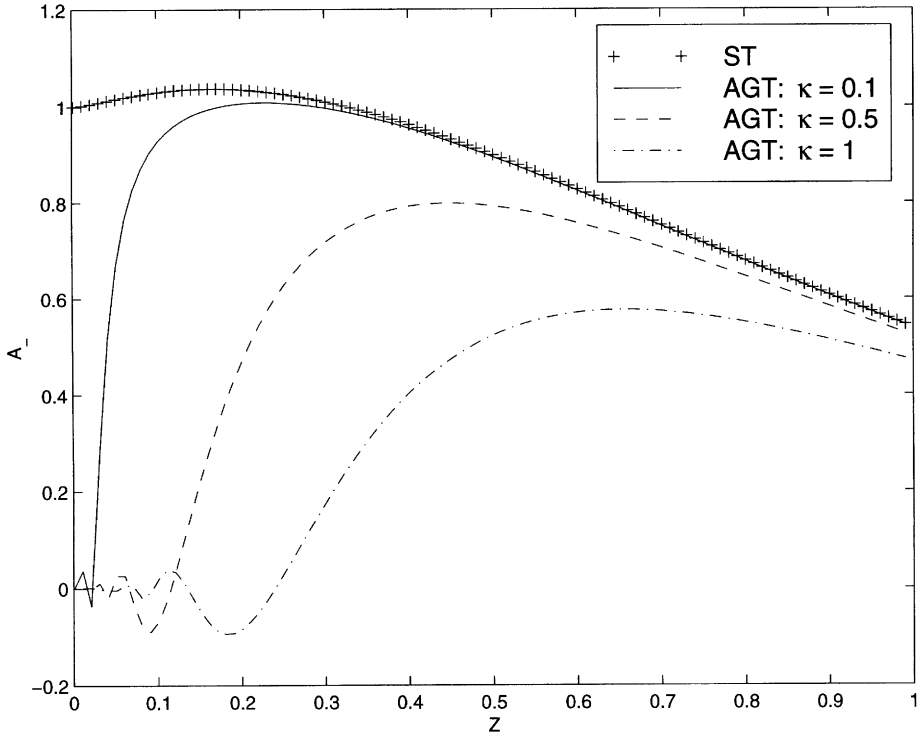

Fig. 1. Comparison of the width function $A^{\mathrm{ST}}(Z)$ of the Standard Theories with the width function A_- of the Advanced Generalized Theory for several values of the parameter

$$\kappa = \frac{9}{2}\left(\frac{\hbar}{m_e v_e}\right)^2 n(nq - n'q')F.$$

As in the ST, we break C functions into real and imaginary parts:

$$C_{\pm,\times}(\chi, Y, Z) \equiv A_{\pm,\times}(\chi, Y, Z) + iB_{\pm,\times}(\chi, Y, Z). \tag{11}$$

Fig. 1 compares the width functions $A_-(Z)$ of the AGT with $A_-(Z)$ of the ST. As can be seen, the AGT results reduces to the ST for large values of the impact parameters. But for small values for the impact parameters, we see that the two theories differ drastically. The ST is finite at $Z = 0$, and with the subsequent multiplication by the factor of $1/Z$ and integrating over impact parameters, this leads to divergence at $Z = 0$. The AGT, on the other hand, is identically zero at $Z = 0$ and that eliminates the divergence at $Z = 0$ in the subsequent integration over impact parameters (after multiplying by the factor $1/Z$). The behavior of A_- in the AGT for that region is oscillatory and dependent on the parameter κ.

An important question that remained unanswered in the GT but is now answered in the AGT, is the following. The GT eliminated the divergence of the electron impact operator at small impact parameters. The divergence, that was a plague in the ST, was related (but not equivalent) to another deficiency of the ST: the electron broadening functions $C(\rho)$ in the ST, at small impact parameters ρ, violated the unitarity of the scattering matrix $S(\rho)$. In the GT, the divergence was eliminated but

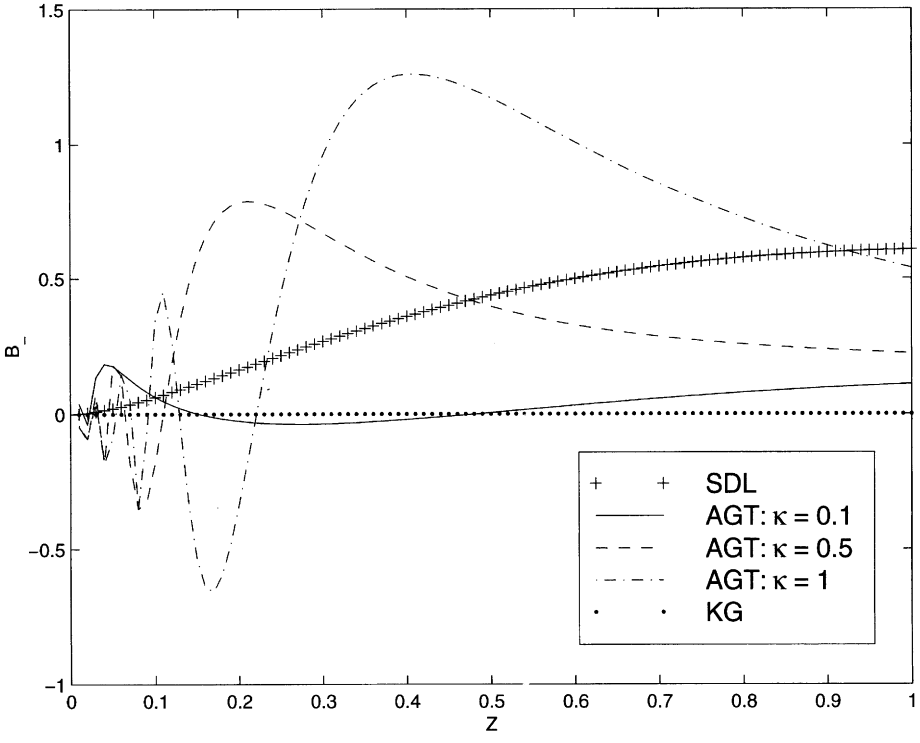

Fig. 2. Comparison of the shift function $B_{-}^{\mathrm{SDL}}(Z)$ of the SDL's theory, the shift function $B_{-}^{\mathrm{KG}}(Z) \equiv 0$ of KG' theory with the shift function B_{-} of the Advanced Generalized Theory for several values of the parameter $\kappa = \frac{9}{2}\left(\frac{\hbar}{m_e v_e}\right)^2 n(nq - n'q')F$.

it remained unclear, whether or not the functions $C(\rho)$ in the GT obey the restrictions imposed by the unitarity of $S(\rho)$.

In the AGT we have shown that for the overwhelming majority of Stark components of hydrogen lines, the functions $C(\rho)$ indeed obey the unitarity restrictions (see Appendix B). This is the next most important physical advantage of the AGT (and GT) over the ST.

Fig. 2 compares the shift functions $B_{-}(Z)$ of the AGT with the corresponding shift functions of KG and SDL. As can be seen the behaviors of all three functions are very different. KG's choice for the shift function was identically zero for all values of the impact parameter: $B_{-}^{\mathrm{KG}} \equiv 0$. As for the AGT's and SDL's, both functions coincide at large values of the impact parameter while the behavior is dramatically different at small impact parameter: SDL's is a smooth curve that increases from zero while that AGT's starts from zero and oscillates at small impact parameters and those oscillations increase with κ.

The next step is to integrate over the impact parameters and is the following:

$$c_{\pm,\times} \equiv \int_0^{\infty} \frac{C_{\pm,\times}\,\mathrm{d}Z}{Z}. \tag{12}$$

Again, as in the ST, we break the c functions into real and imaginary parts:

$$c_{\pm,\times}(\chi, Y, Z) \equiv a_{\pm,\times}(\chi, Y, Z) + \mathrm{i}b_{\pm,\times}(\chi, Y, Z). \tag{13}$$

In the AGT, due to our expansion in terms of χ, we have the imaginary parts of the functions C_+ and $C_\times$ identically zeros:

$$B_+ \equiv B_\times \equiv 0, \tag{14}$$

just like in the standard theories. Thus, we will only describe results for the following broadening functions: $a_{\pm,\times}$ and b_-. Below we present a summary of the final analytical results, referring for details of the derivations to Ref. [4].

2.1. The width function

We have two expressions for the width function a_-: one for the lateral components denoted as a_-^{L} and one for the central components denoted as a_-^{C}.

Before we introduce the expressions for a_-^{L} and a_-^{C}, we present an expression common to both

$$a_-^{\mathrm{AP}}(x,\kappa) = \frac{\sin x}{x^3} - \frac{\cos x}{x^2} + \frac{\sin x}{x} - \mathrm{Ci}x + \frac{\kappa^2\Omega^-}{5}\left[-3\frac{\sin x}{x^5} + 3\frac{\cos x}{x^4} + 4\frac{\sin x}{x^3} + 2\frac{\cos x}{x^2} - 2\frac{\sin x}{x} + \ + 2\mathrm{Ci}\ x \right]$$

where

$$\Omega^- = (\Psi^- + \gamma - \frac{4}{3})(1 - \mathrm{e}^{-Z_D^{10}}) + \left(\Psi^- + 2\gamma - \ln 2 - \frac{4}{3}\right)\frac{\mathrm{e}^{-Z_D^{10}}}{Z_D^2},$$

$$\Psi^- = 0.871250, \qquad \gamma = 0.577216.$$

a_- for the lateral components:

$$a_-^{\mathrm{L}} = \mathrm{e}^{-\alpha\kappa^2} a_-^{\mathrm{AP}}(g,\kappa) + \frac{3\pi^2}{64\kappa}(1 - \mathrm{e}^{-\alpha\kappa^2})$$

where

$$\alpha = 0.211427,$$

$$\kappa = 2|\chi|Y = \frac{\rho_{\mathrm{W}}^{ad}}{\rho_S},$$

$$g = \frac{\kappa}{Z_{\max}} = \frac{2|\chi|Y}{Z_{\max}},$$

$$Z_{\max} = \min(1, Z_D) \approx (1 + Z_D^{-10})^{-1/10}.$$

a_- for the central components:

$$a_-^{\mathrm{C}} = \mathrm{e}^{-\beta\kappa_{\mathrm{C}}^2} a_-^{\mathrm{AP}}(g_C,\kappa_{\mathrm{C}}) + \frac{\eta_0^{2/3}\pi^{4/3}(2/\pi^2 + 1/16)}{\kappa_{\mathrm{C}}^{2/3}}(1 - \mathrm{e}^{-\beta\kappa_{\mathrm{C}}^2})$$

where

$$\beta \equiv 2.7383, \qquad \eta_0 \equiv 0.68595,$$

$$\kappa_{\mathrm{C}} = \eta_0 Y \sqrt{\frac{n^2 - m^2 - 1}{3}},$$

$$g_C = \frac{\kappa_{\mathrm{C}}}{Z_{\max}} = \frac{\eta_0 Y}{Z_{\max}} \sqrt{\frac{n^2 - m^2 - 1}{3}},$$

$$Z_{\max} = \min(1, Z_D) \approx (1 + Z_D^{-10})^{-1/10}.$$

2.2. The coupling function

We have two expressions for the coupling function a_+: one for the lateral components denoted as a_+^{L} and one for the central components denoted as a_+^{C}.

Before we present the expressions for a_+^{L} and a_+^{C}, we present an expression common to both:

$$a_+^{\mathrm{AP}}(x, \kappa) = \frac{\sin x}{x^3} - \frac{\cos x}{x^2} + \frac{\sin x}{x} - \mathrm{Ci}\, x + \frac{\kappa^2 \Omega^+}{5} \left[-3\frac{\sin x}{x^5} + 3\frac{\cos x}{x^4} + 4\frac{\sin x}{x^3} + 2\frac{\cos x}{x^2} - 2\frac{\sin x}{x} + 2\mathrm{Ci}\, x \right]$$

where

$$\Omega^+ = \left(\Psi^+ + \gamma - \frac{4}{3}\right)(1 - \mathrm{e}^{-Z_D^{10}}) + \left(\Psi^+ + 2\gamma - \ln 2 - \frac{4}{3}\right)\frac{\mathrm{e}^{-Z_D^{10}}}{Z_D^2},$$

$$\Psi^+ = -0.125314, \quad \gamma = 0.577216.$$

a_+ for lateral components:

$$a_+^{\mathrm{L}} = a_+^{\mathrm{AP}}(g, \kappa)$$

where

$$\kappa = 2|\chi| Y = \frac{\rho_{\mathrm{W}}^{ad}}{\rho_S},$$

$$g = \frac{\kappa}{Z_{\max}} = \frac{2|\chi| Y}{Z_{\max}},$$

$$Z_{\max} = \min(1, Z_D) \approx (1 + Z_D^{-10})^{-1/10}.$$

a_+ for central components:

$$a_+^{\mathrm{C}} = a_+^{\mathrm{AP}}(g_{\mathrm{C}}, \kappa_{\mathrm{C}})$$

where

$$\eta_0 \equiv 0.68595,$$

$$\kappa_C = \eta_0 Y \sqrt{\frac{n^2 - m^2 - 1}{3}},$$

$$g_C = \frac{\kappa_C}{Z_{max}} = \frac{\eta_0 Y}{Z_{max}} \sqrt{\frac{n^2 - m^2 - 1}{3}},$$

$$Z_{max} = \min(1, Z_D) \approx (1 + Z_D^{-10})^{-1/10}.$$

2.3. The interference function

The interference function $a_\times$, is divided up into two terms, an even term and an odd term with respect to the inversion of the sign of $\omega_{\alpha\alpha'}\omega_{\beta\beta'}$. The following two expressions, $a_\times^e$ and $a_\times^o$ are common to both the lateral components $a_\times^L$ and for the central components $a_\times^C$. The superscript "e" is to indicate that the function is even with respect to the inversion of the sign of $\omega_{\alpha\alpha'}\omega_{\beta\beta'}$ while the superscript "o" is to indicate that the function is odd with respect to the same inversion.

$$a_\times^e(x, \kappa) = 2\left(\frac{\sin x}{x^3} - \frac{\cos x}{x^2} + \frac{\sin x}{x} - \mathrm{Ci}\, x\right)$$

and

$$a_\times^o(x, \kappa) = \frac{\kappa^2 \delta^\pm}{5N}\left\{ -3\frac{\sin x}{x^5} + 3\frac{\cos x}{x^4} + 4\frac{\sin x}{x^3} + 2\frac{\cos x}{x^2} - 2\frac{\sin x}{x} + 2\mathrm{Ci}\, x\right\}$$

where

$$N = n/n' = n_\alpha/n_\beta,$$

$$\delta^+(N) = \left(\Gamma^+ + N\left(2\gamma - \frac{8}{3}\right)\right)(1 - e^{-Z_D^{10}}) + \left(\Gamma^+ + N\left(4\gamma - 2\ln 2 - \frac{2}{N+1}\ln N - \frac{8}{3}\right)\right)\frac{e^{-Z_D^{10}}}{Z_D^2},$$

$$\delta^-(N) = -\left(\Gamma^- + N\left(2\gamma - \frac{8}{3}\right)\right)(1 - e^{-Z_D^{10}}) - \left(\Gamma^- + N\left(4\gamma - 2\ln 2 + \frac{2}{N-1}\ln N - \frac{8}{3}\right)\right)\frac{e^{-Z_D^{10}}}{Z_D^2},$$

$$\Gamma^+ = [-1.695 + 3.439N^{0.830}](1 - e^{-(10/N)^5}) + [0.2290 + 2.562N^{0.921}]e^{-(10/N)^5},$$

$$\Gamma^- = [-0.9474 + 0.6926N^{1.308}](1 - e^{-(10/N)^5}) + [-2.466 + 1.284N^{1.064}]e^{-(10/N)^5}.$$

The superscripts on the expressions for δ are used as follows: δ^+ is used when $\mathrm{sign}(\omega_{\alpha\alpha'}\omega_{\beta\beta'}) = +1$ and δ^- is used when $\mathrm{sign}(\omega_{\alpha\alpha'}\omega_{\beta\beta'}) = -1$.

$a_\times$ for *lateral components*:

$$a^{\mathrm{L}}_\times(\xi,\kappa_\alpha) = a^{\mathrm{e}}_\times(\xi,\kappa_\alpha) + \mathrm{sign}(\omega_{\alpha\alpha'}\omega_{\beta\beta'})a^{\mathrm{o}}_\times(\xi,\kappa_\alpha)$$

where

$$\xi \equiv \kappa_\alpha/Z_{\max} = 2|\chi_\alpha|Y_\alpha/Z_{\max}.$$

$a_\times$ *for central components*:

$$a^{\mathrm{C}}_\times(\xi_{\mathrm{C}},\kappa^{\mathrm{C}}_\alpha) = a^{\mathrm{e}}_\times(\xi_{\mathrm{C}},\kappa^{\mathrm{C}}_\alpha) + \mathrm{sign}(\omega_{\alpha\alpha'}\omega_{\beta\beta'})a^{\mathrm{o}}_\times(\xi_{\mathrm{C}},\kappa^{\mathrm{C}}_\alpha)$$

where

$$\xi_{\mathrm{C}} \equiv \kappa^{\mathrm{C}}_\alpha/Z_{\max},$$

$$\kappa^{\mathrm{C}}_\alpha = \eta_0 Y_\alpha\sqrt{\frac{n^2-m^2-1}{3}},$$

$$\eta_0 \equiv 0.68595.$$

2.4. The shift function

We compute the shift function b_- only for the lateral components. For the central components, b_- enters the impact broadening operator in combination with qn^2 or $q'n'^2$ which are zero for the central components. Therefore, we do not need to compute b_- for the central components, and thus we drop the subscript L from the following expressions for b_- calculated for the lateral components.

$$b_- = \mathrm{sign}(\omega_{\alpha\alpha'})\left[\mathrm{e}^{-\beta\kappa^2}b^{\mathrm{AP}}_-(g) + \frac{3\pi^2}{64\kappa}(1-\mathrm{e}^{-\alpha\kappa^2})\right]$$

where

$$\beta = 0.1, \quad \alpha = 0.001, \quad g = \kappa/Z_{\max}$$

$$\begin{aligned} b^{\mathrm{AP}}_-(x) = {} & \frac{3\pi\kappa}{32}\left[6\frac{\sin x}{x^4} - 6\frac{\cos x}{x^3} - \frac{\sin x}{x^2} - \frac{\cos x}{x} - \mathrm{Si}\,x + \frac{\pi}{2}\right] - \frac{\pi\kappa^2 K_1(Z_0)I_1(Z_0)}{10} \\ & \times\left[6\frac{\sin x}{x^5} - 6\frac{\cos x}{x^4} + 2\frac{\sin x}{x^3} + \frac{\cos x}{x^2} - \frac{\sin x}{x} + \mathrm{Ci}\,x\right] + \frac{\pi\kappa^2 K_0(Z_1)I_0(Z_1)}{10} \\ & \times\left[-3\frac{\sin x}{x^5} + 3\frac{\cos x}{x^4} + 4\frac{\sin x}{x^3} + 2\frac{\cos x}{x^2} - 2\frac{\sin x}{x} + 2\mathrm{Ci}\,x\right] \\ & + \left[\frac{\pi}{2} - \pi Z_{\max}K_0(Z_{\max})I_1(Z_{\max})\right]\Theta(Z_D - Z_C). \end{aligned}$$

Here $K_0(Z)$ and $I_1(Z)$ are the modified Bessel functions of two different kinds,

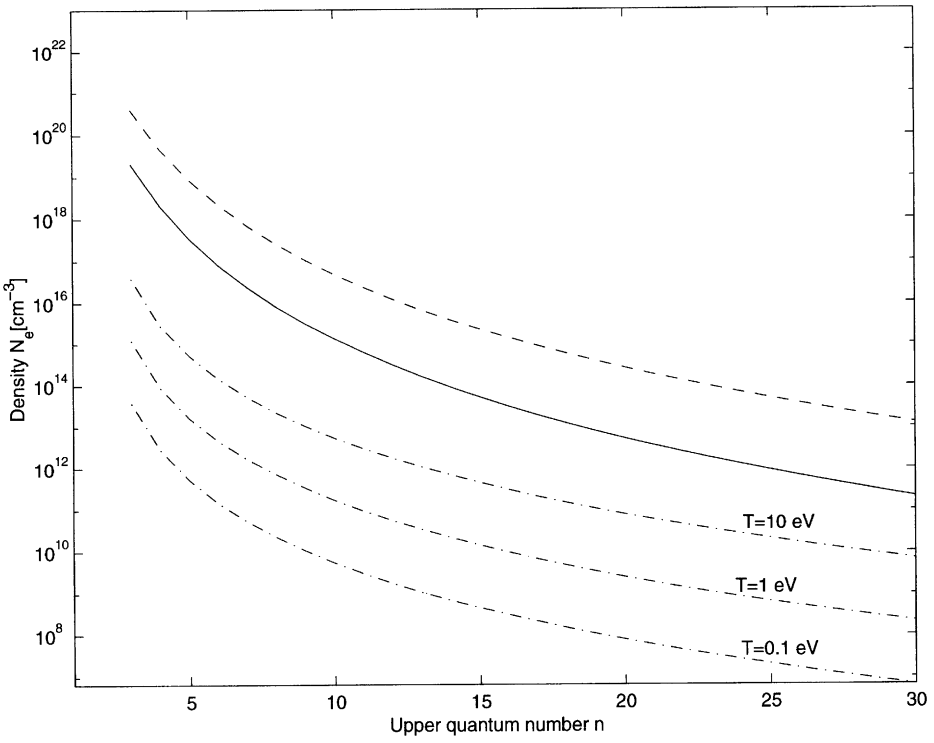

Fig. 3. Applicability range of the AGT. For a given temperature, say 1 eV, the AGT is not valid in the region below the corresponding dash-dotted curve. The solid line acts as a boundary above which the static splitting is much smaller than the plasma electron frequency. The top most line (dashed) is the well known Inglis-Teller limit above which spectral lines merge into a quasi-continuum. In the band between a particular dash-dotted line and the solid line, we expect a dramatic difference between the AGT and the ST. In the band between the solid curve and the dashed curve, the difference between the AGT and the ST should be less significant, but the AGT is still more accurate than the ST.

$$Z_{\max} = \min(Z_C, Z_D) \approx (Z_C^{-10} + Z_D^{-10})^{-1/10}, \quad Z_0 = 0.1785\kappa, \quad Z_1 = 0.2525\kappa,$$
$$Z_c = \kappa^{0.47}/4, \quad \kappa = 2|\chi|Y.$$

Now we discuss the applicability range of the AGT. Fig. 3 shows the electron density N_e plotted against the upper principal quantum number n for Balmer lines. The lower three curves (dash-dotted): defined by Eq. (15), give a lower limit on the electron density: for a given temperature, say 1 eV, the AGT is not valid in the region below this line since the ions in that region are no longer quasi-static:

$$N_e > N_e^{cr} = \frac{1.52 \times 10^{17}\ \text{cm}^{-3}}{(n^2 - n'^2)^3 Z_i^2} \left[\frac{T_i(\text{eV})}{(\mu/M_p)}\right]^{3/2}. \tag{15}$$

The solid line is the boundary above which the static splitting is much smaller than the plasma electron frequency. The curve is described by the following equation:

$$N_e = 1/16\pi a_0^3 n^8. \tag{16}$$

The top most line (dashed) is the well known Inglis–Teller limit above which spectral lines merge into a quasi-continuum. It is described by

$$N_e^{max} = \frac{1}{(12.66\, a_0^2\, n^5)^{3/2}} = \frac{1.50 \times 10^{23}\ \mathrm{cm}^{-3}}{n^{15/2}}. \tag{17}$$

In the band between a particular dash-dotted line and the solid line, we expect a dramatic difference between the AGT and the ST. The difference between the two should become greater as we increase the electron density (as we get closer to the solid curve). In the band between the solid curve and the dashed curve, the difference between the AGT and the ST should be less significant.

3. Tables of Stark width and the physics behind the differences between the AGT and the ST width

We used the AGT to calculate Stark widths for the Lyman and Balmer lines up to the principal quantum number $n = 16$ for broad ranges of electron densities $N_e = 10^{13}$–10^{20} cm^{-3} and temperatures $T = (5\text{–}40) \times 10^3$ K. The tables are presented in Appendix C. The first column is T in units of 10^3 K. The second column is $P = \log[N_e(\mathrm{cm}^3)]$. The next column is the FWHM by the AGT in α-units (Å/CGSE). For the lines which the FWHM by the KG code is available, it is presented in the last column in the last column in α-units. We now compare, where applicable, the AGT with the KG widths.

For some lines, KG *overestimates* the width as compared to the AGT width. While for lines without unshifted components, KG overestimates the width by a relatively small percentage (e.g. by up to 7% for H_β and L_β), the overestimation significantly increases for the H_α line which has unshifted components. For this line, which is the most intensive hydrogen line in the visible range and thus the most important for practical applications, KG overestimates the width by up to 46%.

For the majority of lines, KG *underestimates* the width compared to the AGT width. Even for lines without the unshifted components, the underestimation is quite significant (e.g. by up to 20–21% for H_δ and L_δ). But for the lines with unshifted components, the underestimation is *extremely dramatic*. Indeed, KG unerestimates the width of L_γ by up to 2.8 times, the width of L_α by up to 2.5 times, and the width of H_γ by up to 2 times !

We emphasize that the above dramatic or significant differences would still remain dramatic or significant even after the allowance for Doppler broadening. Therefore it should be of a great practical importance to use the AGT widths rather than the KG widths.

For L_α we can also compare the results of both theories with Grutzmacher's and Wende's experiment [5]. Table 16 shows a comparison between the Stark width obtained by the AGT, KG and the experiment. For the lowest density point $N_e = 10^{17}$ cm^{-3}, the discrepancy of the KG's and AGT's width with the experiment's are about 78% and 55%, respectively. When the initial density is doubled, the discrepancy of the KG's is reduced to about 68% while KG's reduces to 43%. When the initial density is tripled, the discrepancy of the KG's is reduced to about 64% while the AGT's was dramatically reduced to about 35%. Even when the initial density is quadruple, the discrepancy of KG's code is about 62% while the AGT's is just above 31%.

The conventional explanation of the discrepancy between the KG results and experiment was that it was primarily due to the ion dynamics, which was not included in KG code. But as we just

saw, much of this discrepancy was eliminated by a more accurate treatment of the electron field in the AGT without the introduction of ion dynamics. Another conclusion from the same is the following. Those broadening theories that "married" some modeling of the ion dynamics with the conventional (a-la KG) treatment of electrons and obtained an "agreement" with Grutzmacher's and Wende's experiment, had significantly overestimated the actual ion-dynamical contribution.

For most lines, the trend is not so clear. For a particular line, say, KG overestimates the width for some plasma parameters while for another set of plasma parameters, they underestimate the width of the same line relative to the AGT.

These features could be explained by comparing the assumptions and empirical choices that were made by KG with the corresponding, exact-analytically derived, physical characteristics and parameters obtained by the AGT. The main reason that KG code overestimates the width for some spectral lines is presented in the next paragraph.

Kepple–Griem empirically chosen the lower cutoff for the impact parameters (also known as the Weisskopf radius) as

$$\rho_{\mathrm{W}} = \frac{(n^2 - n'^2)}{m_{\mathrm{e}} v_{\mathrm{e}}} \hbar$$

and used this same value for all Stark components of a spectral line, whereas in the AGT, the effective ρ_{W} turns out to be intrinsically individual for each Stark component

$$\rho_{\mathrm{W}}^{\mathrm{AGT}} = 3X\hbar/m_{\mathrm{e}} v_{\mathrm{e}}.$$

In distinction to the KG, the AGT does *not* introduce any empirical lower cutoff. In the AGT results, that are rigorously derived from first principles, we can identify, what plays the role of the Weisskopf radius. That is what the above expression represents. Our calculations (Appendix A) show that the value of the effective $\rho_{\mathrm{W}}^{\mathrm{AGT}} = 3X\hbar/(m_{\mathrm{e}} v_{\mathrm{e}})$ averaged over all Stark component of a hydrogen line is:

- 1.5 times greater than the KG semi-empirical choice of $\rho_{\mathrm{W}}^{\mathrm{KG}} = (n^2 - n'^2)\hbar/(m_{\mathrm{e}} v_{\mathrm{e}})$ for all hydrogen lines that do not have the central components (such as L_β, L_δ, H_β, H_δ, ...),
- approximately 1.5 times greater than the KG semi-empirical choice of $\rho_{\mathrm{W}}^{\mathrm{KG}} = (n^2 - n'^2)\hbar/(m_{\mathrm{e}} v_{\mathrm{e}})$ for most hydrogen lines that do have the central components.

It is this underestimation by KG of the effective Weisskopf radius translates into their overestimation of the width of lines.

For some lines, the following factors enter the game and result in the underestimation of the width by KG.

1. Kepple–Griem had empirically chosen the ion-field-dependent upper cutoff $\rho_{\max}$ as being proportional to $1/n^2$

$$\rho_{\max} \approx \frac{1}{5} \frac{v\hbar}{n^2 \mathrm{e}^2 a_0} N_{\mathrm{e}}^{-2/3}.$$

Table 1
Ratio of the Weisskopf radii of the AGT and the ST

Line	R	Line	R
L_α	1.0400	H_α	1.1159
L_γ	1.5447	H_γ	1.5246
L_6	1.5565	H_7	1.5345
L_8	1.5509	H_9	1.5314
L_{10}	1.5445	H_{11}	1.5278
L_{12}	1.5392	H_{13}	1.5246
L_{14}	1.5349	H_{15}	1.5220
L_{16}	1.5313	H_{17}	1.5198

However, from selection rules for the parabolic quantization, $\rho_{\max}$ should be proportional to $1/n$ (as in the SDL and the AGT)

$$\rho_{\max} \approx \frac{v\hbar}{6.3ne^2a_0} N_e^{-2/3}.$$

2. In the KG and SDL, the dependence on the ion field F entered only the argument of the logarithm (which means a very weak coupling between the ion and electron broadening). In distinction to this, the AGT proves rigorously that the coupling between the ion and electron broadening, which is effective at the high n and/or high N_e ranges, is significantly stronger than it was empirically introduced by both KG and SDL. The strong coupling results in a much slower falloff of the width (a_-) and shift (b_-) functions at large F, than in the KG and SDL.

$$b_-^{\mathrm{AGT}} = a_-^{\mathrm{AGT}} = \frac{3\pi^2}{64\kappa} \quad \text{at } F \gg \frac{2e}{nX}\left(\frac{m_e v_e}{\hbar}\right)^2,$$

$$\kappa = \frac{1}{2e}\left(\frac{\hbar}{m_e v_e}\right)^2 nXF,$$

$$b_-^{\mathrm{ST}} = a_-^{\mathrm{ST}} = 0 \quad \text{at } F \gg \frac{2e}{nX}\left(\frac{m_e v_e}{\hbar}\right)^2.$$

3. Kepple–Griem equates the width (a_-) and coupling (a_+) functions, whereas in the AGT, the width function is always greater than the coupling function. The coupling function acts to reduce the width of the line. Therefore, KG, by setting $a_- \equiv a_+$ (what is incorrect), obtained a smaller width than seen by the AGT.
4. In both the KG and SDL, the choice of the "*strong collision constant*" was empirical and ambiguous.

$$a_- \approx 0.25 + \ln\left(\frac{\rho_D}{\rho_W}\right) \quad \text{KG},$$

$$a_- \approx 0.50 + \ln\left(\frac{\rho_D}{\rho_W}\right) \quad \text{SDL}.$$

Table 2
Stark FWHM of Lyman alpha (1–2)

T	P	AGT	KG
5	16	2.14E − 04	1.66E − 04
5	17	3.74E − 04	2.66E − 04
5	18	5.74E − 04	3.42E − 04
5	19	7.40E − 04	2.94E − 04
10	16	1.65E − 04	1.33E − 04
10	17	2.96E − 04	2.26E − 04
10	18	5.01E − 04	3.44E − 04
10	19	7.28E − 04	3.88E − 04
10	20	8.05E − 04	
20	16	1.29E − 04	1.11E − 04
20	17	2.35E − 04	1.97E − 04
20	18	4.17E − 04	3.22E − 04
20	19	6.64E − 04	4.42E − 04
20	20	8.98E − 04	4.54E − 04
30	16	1.12E − 04	1.01E − 04
30	17	2.04E − 04	1.78E − 04
30	18	3.67E − 04	3.02E − 04
30	19	6.14E − 04	4.48E − 04
30	20	8.56E − 04	5.18E − 04
40	16	1.00E − 04	9.40E − 05
40	17	1.85E − 04	1.64E − 04
40	18	3.35E − 04	2.88E − 04
40	19	5.77E − 04	4.46E − 04
40	20	8.41E − 04	5.54E − 04

The AGT brings up a more accurate value of this "constant"

$$a_{-} \approx 1.063 + \ln\left(\frac{\rho_D}{\rho_W^{AGT}}\right).$$

4. Conclusions

We developed a computationally robust version of the Generalized Theory (GT) called the Advanced Generalized Theory (AGT). In distinction to the Standard Theories (ST), where the electrons were treated as the perturbation, both the GT and the AGT take into account exactly,

Table 3
Stark FWHM of Lyman beta (1–3)

T	P	AGT	KG
5	15	4.09E − 03	4.20E − 03
5	16	4.20E − 03	4.28E − 03
5	17	4.20E − 03	4.28E − 03
5	18	3.72E − 03	3.96E − 03
5	19	2.50E − 03	
10	15	4.20E − 03	4.32E − 03
10	16	4.37E − 03	4.46E − 03
10	17	4.54E − 03	4.60E − 03
10	18	4.47E − 03	4.48E − 03
10	19	3.70E − 03	
20	15	4.28E − 03	4.42E − 03
20	16	4.44E − 03	4.56E − 03
20	17	4.69E − 03	4.78E − 03
20	18	4.92E − 03	4.92E − 03
20	19	4.68E − 03	4.70E − 03
30	15	4.29E − 03	4.44E − 03
30	16	4.46E − 03	4.60E − 03
30	17	4.74E − 03	4.84E − 06
30	18	5.06E − 03	5.12E − 03
30	19	5.10E − 03	5.12E − 03
40	15	4.29E − 03	4.46E − 03
40	16	4.46E − 03	4.62E − 03
40	17	4.74E − 03	4.88E − 03
40	18	5.11E − 03	5.22E − 03
40	19	5.31E − 03	5.38E − 03

nonperturbatively one component of the electron field. This is equivalent to the partial summation of the all-order-diagrams in the quantum broadening theory.

Therefore, both the GT and the AGT are intrinsically more accurate than the ST. That is why one of the primary purposes of this paper was a detailed study of physical consequences, resulting from the different approaches of the AGT and of the ST, as well as the inaccuracies and incorrect empirical choices of the ST, by benchmarking the ST to the AGT.

If we would have to select just one, the most distinctive difference in physical consequences of the AGT and the ST, this would be the strong coupling between the electron and ion broadenings. In the ST, the coupling was very weak: indeed the ion field F entered the electron impact operator only in the argument of a logarithm. In the AGT, the electron impact operator, being entangled with the ion field in a much more complicated fashion, demonstrates a strong dependence on the ion field. This is most clearly manifested in the large-F region, where the ST predicts the 100%

Table 4
Stark FWHM of Lyman Gamma (1–4)

T	P	AGT	KG
5	14	1.06E − 03	8.32E − 04
5	15	4.63E − 03	1.64E − 02
5	16	6.34E − 03	4.52E − 03
5	17	6.56E − 03	4.98E − 03
5	18	5.37E − 03	
10	14	7.69E − 04	6.44E − 04
10	15	1.95E − 03	1.23E − 03
10	16	6.20E − 03	3.28E − 03
10	17	7.23E − 03	5.62E − 03
10	18	6.87E − 03	5.36E − 03
20	14	5.74E − 04	5.08E − 04
20	15	1.22E − 03	9.54E − 04
20	16	5.50E − 03	1.98E − 03
20	17	7.40E − 03	5.68E − 03
20	18	8.02E − 03	6.44E − 03
30	14	4.86E − 04	4.50E − 04
30	15	9.93E − 04	8.42E − 04
30	16	4.49E − 03	1.67E − 02
30	17	7.27E − 03	5.44E − 03
30	18	8.34E − 03	6.90E − 03
40	14	4.34E − 04	4.14E − 04
40	15	8.71E − 04	7.68E − 04
40	16	2.46E − 03	1.49E − 03
40	17	7.10E − 03	5.12E − 03
40	18	8.45E − 03	7.16E − 03

depression (disappearance) of the electron impact broadening by the ion field F above some critical field F_{cr}. In distinction, the AGT shows that even at $F > F_{cr}$, there remains a significant electron impact broadening, which diminishes in a relatively slow way (proportional to $1/F$) with the further increase of F.

Next, an important question that remained unanswered in the GT but we answered in the AGT, is the following. The GT eliminated the divergence of the electron impact operator at small impact parameters. The divergence, that was a plague in the ST, was related (but not equivalent) to another deficiency of the ST: the electron broadening functions $C(\rho)$ in the ST, at small impact parameters ρ, violated the unitarity of the scattering matrix $S(\rho)$. In the GT, the divergence was eliminated but it remained unclear, whether or not the functions $C(\rho)$ in the GT obey the restrictions imposed by the unitarity of $S(\rho)$.

Table 5
Stark FWHM of Lyman delta (1–5)

T	P	AGT	KG
5	13	1.08E − 02	
5	14	1.19E − 02	1.20E − 02
5	15	1.32E − 02	1.30E − 02
5	16	1.42E − 02	1.32E − 02
5	17	1.50E − 02	1.19E − 02
10	13	1.05E − 02	
10	14	1.17E − 02	1.19E − 02
10	15	1.30E − 02	1.31E − 02
10	16	1.45E − 02	1.39E − 02
10	17	1.53E − 02	1.37E − 02
20	13	1.02E − 02	
20	14	1.14E − 02	1.02E − 02
20	15	1.27E − 02	1.29E − 02
20	16	1.44E − 02	1.42E − 02
20	17	1.60E − 02	1.49E − 02
30	13	9.99E − 03	
30	14	1.12E − 02	1.13E − 02
30	15	1.26E − 02	1.27E − 02
30	16	1.42E − 02	1.42E − 02
30	17	1.61E − 02	1.56E − 02
40	13	9.85E − 03	
40	14	1.10E − 02	1.13E − 02
40	15	1.24E − 02	1.23E − 02
40	16	1.40E − 02	1.42E − 02
40	17	1.60E − 02	1.56E − 02

In the AGT we have shown that for the overwhelming majority of Stark components of hydrogen lines, the functions $C(\rho)$ indeed obey the unitarity restrictions (see Appendix B). This is another important physical advantage of the AGT (and GT) over the ST.

Based on our closed-form expressions for the width-, shift-, and coupling-broadening functions, we have calculated Stark profiles of the Lyman and Balmer lines up to the upper principal quantum number $n = 16$ for electron densities from $N_e = 10^{13}\ \mathrm{cm}^{-3}$ to $N_e = 10^{20}\ \mathrm{cm}^{-3}$. We have presented here the most comprehensive tables of Stark widths for all those Lyman and Balmer lines, based on the quasistatic approximation for ions and the impact approximation for electrons.

The mathematical simplicity of the AGT results has made it possible to gain a much deeper physical insight into the following important features of the generalized theories that distinguish the AGT/GT from its predecessors and ensure its superior accuracy. In addition to the much stronger coupling (than in the ST), as discussed above, other distinctive features are the

Table 6
AGT Stark width of L_6–L_{10}

T	P	L_6	L_7	L_8	L_9	L_{10}
5	13	1.22E − 02	2.48E − 02	3.18E − 02	4.70E − 02	5.74E − 02
5	14	1.64E − 02	2.80E − 02	3.66E − 02	5.34E − 02	6.55E − 02
5	15	1.90E − 02	3.13E − 02	4.04E − 02	6.50E − 02	7.21E − 02
5	16	1.99E − 02	3.60E − 02	4.07E − 02		
10	13	2.77E − 03	2.40E − 02	2.99E − 02	4.55E − 02	5.52E − 02
10	14	1.53E − 02	2.73E − 02	3.56E − 02	5.20E − 02	6.39E − 02
10	15	1.88E − 02	3.11E − 02	4.06E − 02	6.46E − 02	7.33E − 02
10	16	2.11E − 02	3.42E − 02	4.43E − 02		
20	13	1.65E − 03	2.31E − 02	2.72E − 02	4.36E − 02	5.25E − 02
20	14	1.35E − 02	2.63E − 02	3.41E − 02	4.99E − 02	6.14E − 02
20	15	1.80E − 02	3.02E − 02	3.98E − 02	6.28E − 02	7.16E − 02
20	16	2.12E − 02	4.06E − 02	4.53E − 02		
30	13	1.33E − 03	2.25E − 02	2.51E − 02	4.25E − 02	5.06E − 02
30	14	1.21E − 02	2.56E − 02	3.29E − 02	4.87E − 02	5.96E − 02
30	15	1.73E − 02	2.96E − 02	3.90E − 02	5.65E − 02	7.01E − 02
30	16	2.09E − 02	3.42E − 02	4.50E − 02		
40	13	1.16E − 03	2.20E − 02	2.33E − 02	4.18E − 02	4.91E − 02
40	14	1.09E − 02	2.51E − 02	3.19E − 02	4.77E − 02	5.83E − 02
40	15	1.67E − 02	2.90E − 02	3.82E − 02	5.55E − 02	6.88E − 02
40	16	2.06E − 02	3.37E − 02	4.45E − 02		

following. Empirical choices of important characteristic impact parameters are now determined more precisely:

1. In the AGT, the effective Weisskopf radius ρ_W is proportional to n^2, while SDL had empirically chosen ρ_W proportional to n.
2. In the AGT, the effective Weisskopf radius ρ_W turns depends on each Stark component (i.e., it is dependent on q), while in KG it was not.
3. In the AGT, the ion-field-dependent upper cutoff ρ_F is proportional to $1/n$, as follows from the selectrion rules for the parabolic quantization, while KG had empirically chosen an expression for ρ_F proportional to $1/n^2$.

Even in the low field and/or density range, where the coupling between the ions and electrons broadening is negligible, the results of the AGT should be more accurate than the results of the Standard Theories. The Weisskopf radius and the "strong collision constant" are derived consistently in the AGT in distinction to both KG and SDL.

Table 7
AGT Stark width of L_{11}–L_{13}

T	P	L_{11}	L_{12}	L_{13}
5	13	7.78E − 02	9.22E − 02	1.29E − 01
5	14	9.72E − 02	1.06E − 01	1.51E − 01
10	13	7.50E − 02	8.86E − 02	1.31E − 01
10	14	9.42E − 02	1.03E − 01	1.46E − 01
20	13	7.17E − 02	8.44E − 02	1.08E − 01
20	14	8.29E − 02	9.91E − 02	1.39E − 01
30	13	6.98E − 02	8.18E − 02	1.05E − 01
30	14	8.05E − 02	9.60E − 02	1.23E − 01
40	13	6.85E − 02	8.00E − 02	1.03E − 01
40	14	7.88E − 02	9.39E − 02	1.20E − 01

Table 8
AGT Stark width of L_{14}–L_{16}

T	P	L_{14}	L_{15}	L_{16}
5	13	1.38E − 01	1.88E − 01	1.97E − 01
10	13	1.32E − 01	1.79E − 01	1.87E − 01
20	13	1.25E − 01	1.55E − 01	1.77E − 01
30	13	1.21E − 01	1.50E − 01	1.71E − 01
40	13	1.19E − 01	1.46E − 01	1.66E − 01

The comparison of the tabulated Stark widths with the KG Stark widths (where applicable) shows the inaccuracy of the latter significantly increases with the growth of both the electron density N_e and the upper principal quantum number n. However, even for the L_α line at densities of the order of 10^{17} cm^{-3}, where the experimental width is by a factor of two greater than the KG width and the entire difference between the two widths was usually "blamed" on the ion dynamics, it turns out the following: the AGT eliminates about one half of this discrepancy just by treating electrons more accurately than in the KG theory, which might mean that the ion-dynamical contribution could be about a factor of two smaller than it was previously thought.

Appendix A. The ratio of the AGT to the ST Weisskopf radius for hydrogen lines

During our analysis, we found that the weighted average over the normalized Stark components for hydrogen lines

$$g_{n,n'} \equiv \sum_X f_X |X| \tag{A.1}$$

Table 9
Stark FWHM of Balmer alpha (2–3)

T	P	AGT	KG
5	15	1.55E − 02	1.94E − 02
5	16	2.16E − 02	2.98E − 02
5	17	3.08E − 02	3.78E − 02
5	18	4.21E − 02	
5	19	5.72E − 02	
10	15	1.36E − 02	1.55E − 02
10	16	1.94E − 02	2.68E − 02
10	17	2.77E − 02	3.72E − 02
10	18	3.93E − 02	4.30E − 02
10	19	5.58E − 02	
20	15	1.15E − 02	1.20E − 02
20	16	1.73E − 02	2.28E − 02
20	17	2.44E − 02	3.50E − 02
20	18	3.59E − 02	4.52E − 02
20	19	5.02E − 02	4.70E − 02
30	15	1.01E − 02	9.96E − 03
30	16	1.61E − 02	2.00E − 02
30	17	2.27E − 02	3.32E − 02
30	18	3.34E − 02	4.50E − 02
30	19	4.81E − 02	5.14E − 02
40	15	9.15E − 03	9.00E − 03
40	16	1.51E − 02	1.84E − 02
40	17	2.16E − 02	3.16E − 02
40	18	3.16E − 02	4.46E − 02
40	19	4.66E − 02	5.38E − 02

could be obtained analytically. For the lines without the central components (i.e., $n + n'$ is even):

$$g_{n,n'} = \tfrac{1}{2}(n^2 - n'^2). \tag{A.2}$$

For the lines with the central components (i.e., $n + n'$ is odd):

$$g_{n,n'} \approx \tfrac{1}{2}n^2,\ n \gg n'; \qquad g_{n,n'} = \tfrac{1}{3}(n^2 - n'^2),\ n = (n' + 1) \gg 1. \tag{A.3}$$

A direct consequence of this result is the ratio of the Weisskopf radius, averaged over all components, of AGT to the semi-empirical Weisskopf radius of KG, is exactly 1.5 for the lines without the central components while it approaches 1.5 for the lines with the central components. Table 1 illustrates that ratio for the lines with the central components, where the ratio R is

$$R \equiv \frac{\langle \rho_{\mathrm{W}}^{\mathrm{AGT}} \rangle}{\rho_{\mathrm{W}}^{\mathrm{ST}}} = 3\frac{\sum_X f_X |X|}{n^2 - n'^2}. \tag{A.4}$$

Table 10
Stark FWHM of Balmer beta (2–4)

T	P	AGT	KG
5	14	1.44E − 01	1.52E − 01
5	15	1.49E − 01	1.57E − 01
5	16	1.56E − 01	1.62E − 01
5	17	1.54E − 01	1.53E − 01
5	18	1.52E − 01	
5	19	1.58E − 01	
10	14	1.47E − 01	1.55E − 01
10	15	1.52E − 01	1.61E − 01
10	16	1.61E − 01	1.68E − 01
10	17	1.69E − 01	1.70E − 01
10	18	1.61E − 01	1.56E − 01
10	19	1.67E − 01	
20	14	1.48E − 01	1.55E − 01
20	15	1.53E − 01	1.63E − 01
20	16	1.62E − 01	1.72E − 01
20	17	1.75E − 01	1.84E − 01
20	18	1.82E − 01	1.79E − 01
20	19	2.08E − 01	
30	14	1.48E − 01	1.58E − 01
30	15	1.53E − 01	1.63E − 01
30	16	1.62E − 01	1.72E − 01
30	17	1.76E − 01	1.84E − 01
30	18	1.89E − 01	1.89E − 01
30	19	1.90E − 01	
40	14	1.49E − 01	1.58E − 01
40	15	1.53E − 01	1.63E − 01
40	16	1.62E − 01	1.72E − 01
40	17	1.76E − 01	1.85E − 01
40	18	1.91E − 01	1.95E − 01
40	19	1.95E − 01	

The numerical results given in Table 1 can be understood physically as follows. Consider a radiative transition $n \leftrightarrow n'$, where $n \gg n'$. In the upper multiplet, the number of sublevels having a particular value of the electric quantum number q is equal to $(n - q)$. However, due to selection rules with respect to the magnetic quantum number m, only $(n' + 1)$ of them participate in the transition if q is even or only n' of them participate in the transition if q is odd (or even less than n' if $q > n - n'$).

Table 11
Stark FWHM of Balmer gamma (2–5)

T	P	AGT	KG
5	14	1.46E − 01	8.84E − 02
5	15	1.88E − 01	1.72E − 01
5	16	2.10E − 01	1.90E − 01
5	17	2.03E − 01	1.71E − 01
10	14	1.01E − 01	5.08E − 02
10	15	1.81E − 01	1.60E − 01
10	16	2.16E − 01	1.99E − 01
10	17	2.31E − 0	2.02E − 01
20	14	4.32E − 02	3.58E − 02
20	15	1.65E − 01	1.26E − 01
20	16	2.12E − 01	1.98E − 01
20	17	2.44E − 01	2.22E − 01
30	14	3.40E − 02	3.10E − 02
30	15	1.49E − 01	7.64E − 02
30	16	2.06E − 01	1.94E − 01
30	17	2.45E − 01	2.28E − 01
40	14	2.89E − 02	2.80E − 02
40	15	2.89E − 02	6.50E − 02
40	16	2.01E − 01	1.89E − 01
40	17	2.44E − 01	2.32E − 01

Allowing for that, let us calculate the average value of $|q|$, for example for an odd n:

$$\langle |q| \rangle_{\mathrm{rad}} \approx 2\frac{\sum_{k=1}^{(n-1)/2}(2k)(n'+1) + \sum_{k=1}^{(n-1)/2}(2k-1)n'}{2\dfrac{n-1}{2}(2n'+1)}$$

$$= \frac{2(2n'+1)\dfrac{1}{2}\dfrac{n-1}{2}\dfrac{n+1}{2} - n'\dfrac{n-1}{2}}{\dfrac{n-1}{2}(2n'+1)}$$

$$= \frac{n+1}{2} - \frac{n'}{2n'+1} = \frac{n}{2}\left[1 + \frac{1}{(2n'+1)n}\right] \approx \frac{n}{2}. \tag{A.5}$$

A similar calculation of $\langle |q| \rangle$ for an even n yields the same result: $\langle |q| \rangle \approx n/2$.

Table 12
Stark FWHM of Balmer delta (2–6)

T	P	AGT	KG
5	13	2.93E − 01	2.98E − 01
5	14	3.23E − 01	3.22E − 01
5	15	3.59E − 01	3.44E − 01
5	16	3.84E − 01	3.38E − 01
5	17	4.30E − 01	
10	13	2.90E − 01	2.94E − 01
10	14	3.17E − 01	3.20E − 01
10	15	3.57E − 01	3.48E − 01
10	16	3.98E − 01	3.64E − 01
10	17	4.06E − 01	3.24E − 01
20	13	2.85E − 01	2.86E − 01
20	14	3.10E − 01	3.18E − 01
20	15	3.47E − 01	3.48E − 01
20	16	3.96E − 01	3.78E − 01
20	17	4.28E − 01	3.70E − 01
30	13	2.81E − 01	2.84E − 01
30	14	3.05E − 01	3.10E − 01
30	15	3.41E − 01	3.46E − 01
30	16	3.90E − 01	3.80E − 01
30	17	4.38E − 01	
40	13	2.79E − 01	2.82E − 01
40	14	3.01E − 01	3.10E − 01
40	15	3.37E − 01	3.42E − 01
40	16	3.85E − 01	3.82E − 01
40	17	4.38E − 01	

If we would disregard the selection rules and average over all Stark sublevels, we would arrive to a different result:

$$\langle |q| \rangle_{\text{all}} \approx 2\frac{\sum_{k=1}^{n-1} q(n-q)}{n^2}$$

$$= \frac{21}{n2}(n-1)n - \frac{2}{6n^2}(n-1)n(2n-1)$$

$$= (n-1)\frac{n+1}{3n}$$

Table 13
AGT Stark width of H_7–H_{10}

T	P	H_7	H_8	H_9	H_{10}
5	13	3.72E − 01	5.81E − 01	7.33E − 01	1.01E + 00
5	14	4.35E − 01	6.57E − 01	8.30E − 01	1.15E + 00
5	15	4.83E − 01	7.32E − 01	9.13E − 01	1.48E + 00
5	16	4.99E − 01	8.96E − 01		
10	13	3.45E − 01	5.66E − 01	7.08E − 01	9.73E − 01
10	14	4.21E − 01	6.39E − 01	8.11E − 01	1.12E + 00
10	15	4.85E − 01	8.76E − 01	9.23E − 01	1.44E + 00
10	16	5.33E − 01	9.18E − 01		
20	13	3.08E − 01	5.48E − 01	6.72E − 01	9.34E − 01
20	14	3.99E − 01	6.17E − 01	7.82E − 01	1.07E + 00
20	15	4.73E − 01	7.10E − 01	9.04E − 01	1.37E + 00
20	16	5.40E − 01	9.02E − 01		
30	13	2.80E − 01	5.36E − 01	6.47E − 01	9.11E − 01
30	14	3.82E − 01	6.03E − 01	7.61E − 01	1.04E + 00
30	15	4.61E − 01	6.94E − 01	8.85E − 01	1.33E + 00
30	16	5.36E − 01	8.84E − 01		
40	13	2.57E − 01	5.28E − 01	6.27E − 01	8.95E − 01
40	14	3.69E − 01	5.93E − 01	7.46E − 01	1.02E + 00
40	15	4.51E − 01	6.82E − 01	8.69E − 01	1.19E + 00
40	16	5.29E − 01	7.84E − 01		

$$= \frac{n^2 - 1}{3n}$$

$$\approx \frac{n}{3}. \tag{A.6}$$

However, it should be emphasized that averaging over *all* Stark sublevels should be appropriate for $n = n' + 1 \gg 1$, since in this case practically all Stark sublevels of both the upper and lower multiplets are involved in the radiative transition. This expectation is confirmed by our numerical calculations of the quantity $g_{n,n'}$ for $n = n' + 1$. As the result of the numerical calculations in this case we obtained

$$\lim_{n \to \infty} g_{n,n-1} \approx n^2/3, \tag{A.7}$$

which is consistent with the analytical result Eq. (A.6).

Table 14
AGT Stark width of H_{11}–H_{13}

T	P	H_{11}	H_{12}	H_{13}
5	13	1.22E + 00	1.58E + 00	1.86E + 00
5	14	1.39E + 00	2.06E + 00	2.15E + 00
10	13	1.17E + 00	1.52E + 00	1.79E + 00
10	14	1.35E + 00	1.96E + 00	2.09E + 00
20	13	1.12E + 00	1.45E + 00	1.70E + 00
20	14	1.30E + 00	1.85E + 00	2.00E + 00
30	13	1.09E + 00	1.41E + 00	1.65E + 00
30	14	1.26E + 00	1.91E + 00	1.94E + 00
40	13	1.07E + 00	1.38E + 00	1.62E + 00
40	14	1.24E + 00	1.60E + 00	1.89E + 00

Appendix B. Fulfillment of the unitarity requirements at large $|\chi|$

The electron impact operator is given by

$$\phi_{nn'} = N_e \int_0^\infty f(v) v \int_0^\infty d\rho \, 2\pi\rho \{S_n S_{n'}^* - 1\}_{avg}.$$

For the Lyman series:

$$\phi_{nn'} = N_e \int_0^\infty f(v) v \int_0^\infty d\rho \, 2\pi\rho \{S_n - 1\}_{avg}$$

$$= -N_e \int_0^\infty f(v) v \int_0^\infty d\rho \, 2\pi\rho \left\{ \frac{2\hbar^2 \sum_{\alpha'} (|x_{\alpha\alpha'}|^2 + |y_{\alpha\alpha'}|^2)}{3m_e^2 v^2 \rho^2 a_0^2} C \right\}, \tag{B.1}$$

$$C_- = \frac{3m_e^2 v^2 \rho^2 a_0^2}{2\hbar^2 \sum_{\alpha'} (|x_{\alpha\alpha'}|^2 + |y_{\alpha\alpha'}|^2)} \{1 - S_n\}_{av}$$

$$= \frac{4m_e^2 v^2 \rho^2 Z_r^2}{3n^2(n^2 - q^2 - m^2 - 1)\hbar^2} \{1 - S_n\}_{av}. \tag{B.2}$$

Table 15
AGT Stark width of H_{14}–H_{16}

T	P	H_{14}	H_{15}	H_{16}
5	13	2.60E + 00	2.70E + 00	3.72E + 00
10	13	2.44E + 00	2.58E + 00	3.48E + 00
20	13	2.12E + 00	2.44E + 00	3.22E + 00
30	13	2.05E + 00	2.36E + 00	3.08E + 00
40	13	2.01E + 00	2.31E + 00	2.98E + 00

The coefficient in front the $\{\cdots\}$ can be re-written as

$$\frac{4}{3(n^2-q^2-m^2-1)}\frac{\rho^2(3/2)^2}{\left(\frac{3n\hbar}{2Z_r m_e v}\right)^2}=\frac{3}{n^2-q^2-m^2-1}\left(\frac{\rho}{\rho_W^{n.a.}}\right)^2$$

where

$$\rho_W^{n.a.}\equiv\frac{3n\hbar}{2Z_r m_e v}.$$

Since

$$\rho/\rho_W^{n.a.}=Z/Y$$

we get

$$C_-=\frac{3}{n^2-q^2-m^2-1}\left(\frac{Z}{Y}\right)^2\{1-S_n\}_{avg}.$$

By choosing $|1-S_n|=2$, we finally obtain

$$C_-^{u.l.}=\frac{6}{n^2-q^2-m^2-1}\left(\frac{Z}{Y}\right)^2. \tag{B.3}$$

The coefficient in front of Z^2/Y^2 reaches its maximum value for $n=2\Rightarrow$

$$(C_-^{u.l})_{max}=3Z^2/Y^2.$$

Using the results of Appendix A, we now analyze the average of

$$\chi_\alpha=q_\alpha-\frac{n_\beta}{n_\alpha}q_\beta.$$

In the case of $n_\alpha=n_\beta+1\gg1$:

$$\bar{\chi}_\alpha=\bar{q}_\alpha-\frac{n\bar{\beta}}{n_\alpha}\bar{q}_\beta=\frac{n_\alpha^2-1}{3n_\alpha}-\frac{n_\beta}{n_\alpha}\cdot\frac{n_\beta^2-1}{3n_\beta}$$

$$=\frac{n_\alpha^2-n_\beta^2}{3n_\alpha}\approx\frac{n_\alpha}{3}. \tag{B.4}$$

Table 16
Comparison with Grutzmacher–Wende's experiment for Lyman alpha (1–2)

N_e (10^{17} cm^{-3})	$T(K)$	AGT (Å)	KG (Å)	EX (Å)	AGTD (%)	KGD (%)
1	12700	7.382E − 3	5.000E − 3	1.660E − 2	55.53	78.26
2	13200	1.375E − 2	9.500E − 3	2.420E − 2	43.19	68.33
3	13200	1.987E − 2	1.300E − 2	3.050E − 2	34.84	63.89
4	14000	2.537E − 2	1.600E − 3	3.680E − 2	31.06	67.9

In the case of $n_\alpha \gg n_\beta$:

$$\bar{\chi}_\alpha = \bar{q}_\alpha - \frac{n\bar{\beta}}{n_\alpha}\bar{q}_\beta \approx \frac{n_\alpha}{2} - \frac{n_\beta}{n_\alpha}\frac{n_\beta}{2}$$

$$= \frac{n_\alpha^2 - n_\beta^2}{2n_\alpha} \approx \frac{n_\alpha}{2}. \tag{B.5}$$

Here and below the symbol $\bar{f}$ means the average of f over the line space.

$$\overline{(n^2 - q^2 - m^2 - 1)} \approx \frac{2n^2}{3} \qquad (\text{for } n \gg 1 \text{ and for } n = n' + 1 \gg 1)$$

$$\overline{C_-^{\text{u.l.}}} \approx \frac{6Z^2}{2n^2Y^2/3} = \frac{9Z^2}{n^2Y^2} = \begin{cases} (\frac{Z}{\bar{\chi}Y})^2 = (\frac{2Z}{a})^2 & \text{for } n = n' + 1 \gg 1, \\ (\frac{3Z}{2\bar{\chi}Y})^2 = (\frac{3Z}{a})^2 & \text{for } n \gg n', \end{cases}$$

where $a \equiv 2|\chi|Y$. Generalized theory for $|\chi| \gg 1$ at small Z yields

$$\Re C_- \approx -\frac{3Z^2}{a^2}\cos\left(\frac{a}{Z}\right) \Rightarrow |\Re C_-| \leq 3\frac{Z^2}{a^2} < \overline{C_-^{\text{u.l.}}}. \tag{B.6}$$

Appendix C. Lyman and Balmer Stark width tables

In this section we present tables (Tables 2–16) of Stark width for Lyman and Balmer lines up to $n = 16$. We compare with KG[6] (where available). The following is an explanation of the symbols that appear in the tables. The tables are divided into two groups: one group has both the AGT's and KG's results and the other group has only the AGT's (KG's data is not available). Both groups have the first and second columns common. The first column, labeled T, represents the temperature as $10^3 T$ K. The second column, labeled P, represents the electron density as $N_e = 10^P$ cm^{-3}. For the first group, column number three, with the label AGT, represents the FWHM obtained from the AGT profile and last column, represents the FWHM given by KG [6]. Each of the first group tables represent a separate spectral line (tables $L_\alpha - L_\delta$ and $H_\alpha - H_\delta$). The tables of the

second group show the AGT width only, for several lines at a time. All FWHM are in alpha units

$$\lambda_\alpha = \frac{\lambda\ (\text{Å})}{1.2503 \times 10^{-9}[N_e^{2/3}\ (\text{cm}^{-3})]^{2/3}}.$$

Table 16 presents Stark Width produced by the AGT and KG as compared with the Grutzmacher–Wende's experimental width (EX) for the Lyman-Alpha line. AGTD is the discrepancy between the AGT and the experiment, and KGD is the discrepancy between KG and the experiment.

References

[1] Ispolatov Ya, Oks EA. JQSRT 1994 51;129–38.
[2] Kepple P, Griem HR. Phys Rev 1968 173;317–25.
[3] Sholin GV, Demura AV, Lisitsa VS. Sov Phys JETP 1973 37;1057–65.
[4] Touma JE. PhD Thesis, Auburn University, 1998
[5] Grutzmacher K, Wende B. Phys Rev A 1977 16;243.
[6] Griem HR. Spectral line broadening by plasmas. New York: Academic Press, 1974. Appendix III.